



RESEARCH PAPER

A fractional mathematical model approach on glioblastoma growth: tumor visibility timing and patient survival

Nurdan Kar ^{1,*} and Nuri Özalp ^{1,‡}

¹Department of Mathematics, Ankara University, 06100 Ankara, Türkiye

*Corresponding Author

‡ kar@ankara.edu.tr (Nurdan Kar); nozalp@science.ankara.edu.tr (Nuri Özalp)

Abstract

In this paper, we introduce a mathematical model given by

$${}^c \mathcal{D}_t^\alpha u = \nabla \cdot D\nabla u + \rho f(u) \quad \text{in } \Omega, \quad (1)$$

where $f(u) = \frac{1}{1-u/K}$, $u/K \neq 1$, $K > 0$, to enhance established mathematical methodologies for better understanding glioblastoma dynamics at the macroscopic scale. The tumor growth model exhibits an innovative structure even within the conventional framework, including a proliferation term, $f(u)$, presented in a different form compared to existing macroscopic glioblastoma models. Moreover, it represents a further refined model by incorporating a calibration criterion based on the integration of a fractional derivative, α , which differs from the existing models for glioblastoma. Throughout this study, we initially discuss the modeling dynamics of the tumor growth model. Given the frequent recurrence observed in glioblastoma cases, we then track tumor mass formation and provide predictions for tumor visibility timing on medical imaging to elucidate the recurrence periods. Furthermore, we investigate the correlation between tumor growth speed and survival duration to uncover the relationship between these two variables through an experimental approach. To conduct these patient-specific analyses, we employ glioblastoma patient data and present the results via numerical simulations. In conclusion, the findings on tumor visibility timing align with empirical observations, and the investigations into patient survival further corroborate the well-established inter-patient variability for glioblastoma cases.

Keywords: Glioblastoma; tumor visibility; recurrence; survival; fractional mathematical model

AMS 2020 Classification: 35K57; 35K67; 65M06; 92B05; 92C37

1 Introduction

Glioblastoma, an aggressive brain tumor known for its high lethality, exhibits an elusive structure owing to its intricate cellular nature. Due to this challenging cellular architecture and histological

diversity, glioblastomas have long been recognized as exemplars of tumor heterogeneity, earning the appellation "multiforme" [1]. In accordance with the 2021 classification of Central Nervous System (CNS) tumors by the World Health Organization (WHO), glioblastomas are officially categorized as *Isocitrate dehydrogenase* (IDH) wild type, signifying the most aggressive variant among diffuse gliomas [2].

The current therapeutic approaches for glioblastoma include a multimodal strategy involving surgical intervention, radiation therapy, and chemotherapy [3]. The standard treatment protocols for newly diagnosed glioblastoma patients typically begin with a maximally safe resection, followed by a combined treatment phase comprising both radiotherapy and chemotherapy. In the aftermath, a monotherapy phase comprising adjuvant chemotherapy ensues. Unfortunately, despite this intensive treatment schedule and advancements in medical imaging for early glioblastoma detection, instances of recurrence near the resection margin persist [4–6]. Even though chemotherapy appears to be the most efficient way to reach all tumor cells, leading to apparent regression on magnetic resonance imaging (MRI), the extent of tumor spread is almost unaffected due to the continued motility of tumor cells [7]. As a result, extensively invaded tumor cells remain below the detection capabilities of MRI, and recurrences manifest upon treatment cessation. Considering this reality, we delve into an exploration of recurrence periods in a cohort of ten patients as part of this study. By doing this, we aim to predict the timing of tumor visibility on MRI. We consider that there are at least three benefits to this analysis: 1) There may be an opportunity for early detection of tumor recurrence; 2) Understanding recurrence trends may contribute to a more personalized approach to patient care; 3) The focus on predicting tumor visibility on MRI scans may help optimize imaging resources. In conducting this analysis, we take into account the dynamics of the angiogenesis process. Angiogenesis involves the formation of new capillary blood vessels from existing microvessels as well as the differential recruitment of relevant supporting cells to different parts of the vascular system [8]. New blood vessels formed through angiogenesis provide the means for further cell proliferation by ensuring a constant supply of nutrients and oxygen. On the other hand, one of the pathological features that distinguish glioblastoma from low-grade glial tumors is microvascular proliferation [9]. However, T1-weighted MRI with gadolinium contrast (T1Gd) images the abnormally leaky vasculature within the tumor and outlines the bulk of the lesion [10]. Taking into account all these factors and acknowledging a direct correlation between the count of proliferating tumor cells and blood vessels, we produce results regarding the visibility of the tumor by taking the count of glioblastoma cells into consideration. Therefore, we assign all parameter values for the model while considering T1Gd.

The objectives behind mathematically modeling brain tumor growth are multifaceted. These encompass mechanisms for deciphering the regulation of disease progression, adapting models to individual patients, and correlating them with clinically relevant data to gauge tumor occurrences such as recurrence trends, aggressiveness, and treatment response. Unlike microscopic models, which are not suitable for medical images, macroscopic models prove more efficient in capturing the average behavior of tumor cells and modeling the evolution of local tumor cell densities than individual cells [11]. In mathematical models at the macroscopic scale, tumors undergo classification based on their motility, denoting invasiveness, and the rate of cellular division, denoting proliferation, and are typically elucidated through the lens of reaction-diffusion formalism [7, 11–24]. However, it is noteworthy that existing models utilize classical reaction-diffusion approaches, particularly in the context of glioblastoma growth. To the best of our knowledge, fractional reaction-diffusion modeling for glioblastoma growth has not been reported in the literature, despite the increasing prevalence of fractional models for disease modeling [25–29]. In this work, we propose a fractional tumor growth model at a macroscopic scale, rooted in a mathematical problem known as the quenching problem [30], which incorporates a type of

reaction-diffusion equation. In the context of the quenching problem, studies have delved into the global existence of its solutions, and analyses pertaining to quenching and non-quenching scenarios [31–35]. The relationship between quenching and blow-up problems has been another focal point to investigate [36, 37]. This investigation has been extended to parabolic systems, with a specific focus on quenching behavior in the presence of singular multi-nonlinearity [38–42]. More recently, attention has turned towards fractional versions of the problem [43, 44]. This shift is driven by the burgeoning interest in fractional calculus that has evolved over the last few decades. In addition, fractional differential equations have gained significant attention due to their potential applications across diverse areas in science and engineering along with their notable theoretical importance [9, 45–49]. Various definitions of fractional derivatives have been proposed in the literature. Among these, one of the most widely recognized is the Caputo fractional derivative [45, 47, 50, 51], notable for its memory effect. Additionally, it is known that the Caputo fractional derivative becomes equivalent to the conventional derivative as the fractional derivative order approaches a conventional derivative order. Considering all of these, we employ the Caputo derivative within the glioblastoma growth model to discern the memory effect and observe its differences from the classical derivative. We consider that such a selection serves as an appropriate operator for conducting analyses in this work that incorporate temporal assessments. Therefore, we anticipate that a more effective fitting of the growth model to patient data can be achieved by employing the Caputo derivative as a calibration criterion. To build up the growth model, we enhance the conventional framework of the quenching problem to more effectively capture glioblastoma dynamics through tailored modifications. Since temporal considerations are in question here, we first introduce the Caputo fractional derivative to the time-dependent term in the mathematical equation. As a second modification, we incorporate a term that represents the maximum cell carrying capacity of the tissue, K , into the proliferation term, $f(u)$. We consider that this approach offers a more efficient modeling framework, facilitating an investigation into the potential trajectory of tumor cell density over a meaningful time frame.

The subsequent sections of this paper are organized as follows: **Section 2** provides a brief exploration of the theoretical groundwork for the tumor growth model, including properties of the Caputo fractional derivative. **Section 3** presents the tumor growth model, its initialization and implementation along with the numerical scheme. **Section 4** presents key findings, encompassing an exploration of the fundamental dynamics and operational principles of the model, investigations into the timing of tumor visibility in a patient cohort, and an analysis of the relationship between tumor growth speeds and patient survival.

2 Theoretical background

In this section, we provide an overview of the growth model's background and highlight some properties related to the Caputo fractional derivative.

In 1975, Kawarada proposed a one-dimensional initial-boundary-value problem, which is known as the quenching problem, denoted as

$$\begin{cases} u_t(x, t) = u_{xx}(x, t) + \frac{1}{1-u} & \text{in } (0, L) \times (0, T), \\ u(0, t) = u(L, t) = 0 & \text{in } (0, T), \\ u(x, 0) = 0 & \text{on } [0, L], \end{cases} \quad (2)$$

where L is a positive real number indicating the length of spatial domain [30]. Mathematically, a

solution of problem (2) is said to quench if there exists a finite time T such that

$$\lim_{t \rightarrow T^-} \sup\{ |u_t(x, t)| : x \in [0, L] \} \rightarrow \infty. \tag{3}$$

The value of T represents the quenching time. A necessary condition for appearance of quenching is

$$\lim_{t \rightarrow T^-} \max\{ |u(x, t)| : x \in [0, L] \} \rightarrow 1^-. \tag{4}$$

One of the important results for problem (2) is provided by the following lemma.

Lemma 1 [32] *If $T < +\infty$, then there exists $x^* \in [0, L]$ such that*

$$\lim_{(x,t) \rightarrow (x^*, T)} u(x, t) = 1. \tag{5}$$

We now provide the relevant definitions for the Caputo fractional derivative. Let $\Gamma(\cdot)$ be Euler’s gamma function.

Definition 1 [45, page 92] *Let $0 < \alpha < 1$ and $u(x) \in AC[a, b]$. Then the left-sided and right-sided Caputo fractional derivatives of u exist almost everywhere and are respectively defined as*

$$\begin{aligned} ({}^c\mathcal{D}_x^\alpha)(u(x)) &= ({}_aI_x^{1-\alpha}) \frac{du(x)}{dx}, \quad x > a, \\ ({}^c\mathcal{D}_b^\alpha)(u(x)) &= - ({}_xI_b^{1-\alpha}) \frac{du(x)}{dx}, \quad x < b. \end{aligned}$$

The set $AC[a, b]$ denotes the collection of all functions that are absolutely continuous in domain $[a, b]$.

In a similar manner, one can articulate a partial fractional derivative for a function with multiple variables as follows.

Definition 2 [45, page 358] *The Caputo fractional derivative of a function $u(x, t)$, with $0 < \alpha < 1$ denoting the order of the derivative, is defined as*

$$({}^c\mathcal{D}_t^\alpha)(u(x, t)) = \frac{1}{\Gamma(1-\alpha)} \int_0^t (t-s)^{-\alpha} \frac{\partial u(x, s)}{\partial s} ds,$$

where $0 < x < L$ and $t > 0$.

Remark 1 [47, page 79] *If $u(x, t)$ is continuously differentiable on t , then $({}^c\mathcal{D}_t^\alpha)(u(x, t)) \rightarrow \frac{\partial u(x, t)}{\partial t}$ as $\alpha \rightarrow 1$.*

3 Method

In the subsequent part of this section, we present our tumor growth model, its initialization and implementation along with the specified numerical scheme.

Tumor growth model

In this work, we model the spatio-temporal evolution of glioblastoma growth using a time-fractional partial differential equation with $\Omega = (0, L) \times (0, T)$ given by

$$\underbrace{{}^c\mathcal{D}_t^\alpha u}_{\text{the distribution of glioblastoma cell density}} = \underbrace{\nabla \cdot D\nabla u}_{\text{net invasion of glioblastoma cells}} + \underbrace{\rho f(u)}_{\text{net proliferation of glioblastoma cells}} \text{ in } \underbrace{\Omega}_{\text{brain anatomy}}, \quad (6)$$

where α , $0 < \alpha \leq 1$, is the Caputo fractional derivative order, $u = u(t, x, y)$ (*cells/mm³*) is the glioblastoma cell density, D (*mm²/year*) is the net invasion rate, ρ (*1/year*) is the net proliferation rate, and the proliferation term satisfy

$$f(u) = \frac{1}{1 - u/K}, \quad u/K \neq 1, \quad K > 0, \quad (7)$$

where K (*cells/mm³*) is the maximum cell carrying capacity of tissue for tumor cells. The equation (6) can be solved under various dimensional assumptions. Here, we employ a two-dimensional spatial derivative in the equation.

Hypothesis

To provide a theoretical foundation for our findings, we propose the following hypothesis, considering statements (3)-(4) and [Lemma 1](#) given in [Section 2](#).

Hypothesis. If the glioblastoma cell density, u , approaches the maximum cell carrying capacity of the tissue, K

$$u \rightarrow K, \quad K < +\infty, \quad t \rightarrow T, \quad (8)$$

then the distribution of glioblastoma cell density, ${}^c\mathcal{D}_t^\alpha u$, increases

$${}^c\mathcal{D}_t^\alpha u \rightarrow \infty, \quad t \rightarrow T. \quad (9)$$

Then, there exist a critical point (T, x^*, y^*) , such that the glioblastoma cell density, u , reaches the maximum cell carrying capacity of tissue, K

$$\lim_{(t, x, y) \rightarrow (T, x^*, y^*)} u = K, \quad T < +\infty. \quad (10)$$

This allows the model to approximate the critical point at which the glioblastoma cell density reaches the maximum cell carrying capacity of the tissue, K , allowing the examination of the time interval leading to this important event. At this juncture, we make two assumptions: *i*) When the glioblastoma cell density reaches the maximum cell carrying capacity of tissue, K , a critical and lethal cell population becomes detectable on MRI; *ii*) When the glioblastoma cell density reaches the maximum cell carrying capacity of tissue, K , it results in necrosis, detectable through MRI. In both cases, the glioblastoma cell density should become visible at a certain time $t \in (0, T)$ before reaching the maximum cell carrying capacity of the tissue, K . Hence, this implies that equation (6) can serve as a prognostic tool for predicting the timing of tumor visibility.

Note that, given that the model is defined in a closed domain, the statement (9) refers to a growth in the distribution of glioblastoma cell density, ${}^c\mathcal{D}_t^\alpha u$, rather than a true approximation to infinity.

Once the glioblastoma cell density, u , reaches the maximum cell carrying capacity of the tissue, K , in a finite time period $T < +\infty$, the distribution of glioblastoma cell density, ${}^c\mathcal{D}_t^\alpha u$, proceeds over the same time period.

Model initialization and implementation

The complete specification of equation (6) necessitates the inclusion of both initial and boundary conditions. The tumor theoretically begins with a single cancerous cell, but the timing and specifics of its initial growth and spread are unknown. We assume that at the time of diagnosis, any previous, presumably uniform distribution of cells has already been disrupted. Thus, in order to characterize the current behavior of tumor cells, we employ the Gaussian distribution as given by

$$u(0, x, y) = u_0 \exp\left(-\frac{|x - x_0|^2 + |y - y_0|^2}{2\sigma^2}\right) > 0, \tag{11}$$

where u_0 is the initial cell density, σ is the standard deviation, and x_0, y_0 is the peak of the Gaussian distribution. Utilizing such an initial condition, we anticipate that tumor cells exhibit denser clustering around the center of the tumor, gradually decreasing in density as one moves away from the center. We impose a no-flux boundary condition

$$\nabla u \cdot \vec{n} = 0, \quad \text{in } \partial\Omega, \tag{12}$$

where \vec{n} is the outward unit normal to $\partial\Omega$. The skull and ventricles are not invaded by the tumor cells and serve as domain boundaries as indicated by equation (12).

We implement a finite difference scheme to solve the time-fractional equation (6), along with the initial condition (11) and the boundary condition (12), by following [43]. In particular, we employ a numerical scheme that incorporates the Caputo fractional derivative for the time-dependent term along with the two-dimensional space-dependent derivative, as given by

$$\begin{aligned} & \frac{1}{\Gamma(1-\alpha)} \sum_{m=0}^{k-1} \frac{u(t_{m+1}, x_i, y_j) - u(t_m, x_i, y_j)}{\tau} \int_{t_m}^{t_{m+1}} (t_k - s)^{-\alpha} ds \\ &= \text{D} \left\{ \frac{u(t_{k-1}, x_{i-1}, y_j) - 2u(t_{k-1}, x_i, y_j) + u(t_{k-1}, x_{i+1}, y_j)}{\Delta x^2} \right\} \\ &+ \text{D} \left\{ \frac{u(t_{k-1}, x_i, y_{j-1}) - 2u(t_{k-1}, x_i, y_j) + u(t_{k-1}, x_i, y_{j+1})}{\Delta y^2} \right\} + \rho f(u(t_{k-1}, x_i, y_j)), \end{aligned} \tag{13}$$

where the time step size is τ . Accordingly, the temporal nodes are given by $t_k = k\tau, k = 0, 1, \dots, Nt$. Similarly, the spatial nodes are defined as $x_i = i\Delta x, i = 0, 1, \dots, Nx$ with $\Delta x = Lx/Nx$ and $y_j = j\Delta y, j = 0, 1, \dots, Ny$ with $\Delta y = Ly/Ny$, representing the spatial step sizes.

Note that the Caputo fractional derivative, which is given in Definition 2, is applicable only within the order interval of $0 < \alpha < 1$. Thus, incorporating the fractional derivative order of 1 directly into the numerical scheme (13) is not feasible. However, Remark 1 indicates that the Caputo fractional derivative converges toward the classical derivative as the values of α approach 1. This implies that the fractional numerical scheme (13) turns into a classical scheme. Hence, we additionally implement and execute the well-known classical finite difference scheme to conduct comparative assessments in the subsequent parts. We explore the distinctions between

the fractional and classical derivatives by utilizing α values that are smaller and closer to 1.

4 Results

In this section, we first discuss the dynamics of the growth model under different fractional derivative orders of α . We observe that the growth model is characterized by predominant proliferation behavior. Recognizing the potential utility of this outcome as a tool for monitoring tumor mass formation, we proceed to estimate the timing of tumor visibility on MRI for a specified patient cohort. Finally, we analyze the correlation between variations in tumor growth speed and patient survival through an experimental study. For all computational approaches and simulations here, we use Python programming language.

Dominance assessment of proliferation rate

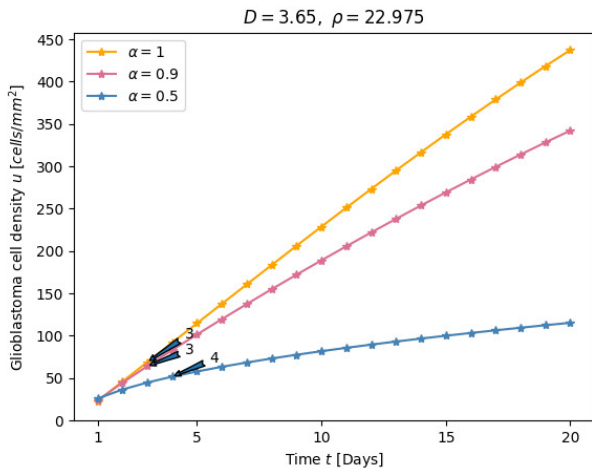
Throughout our investigations, we integrate the parameter values from the existing studies considering T1Gd MRI into our growth model. In this section, we explain the dynamics modeled by equation (6), along with the initial condition (11) and the boundary condition (12), before discussing results on tumor visibility timing. To conduct these analyses, we leverage the numerical data pertaining to invasion, D , and proliferation, ρ , rates for a cohort of glioblastoma patients provided in [52]. These values, estimated from lesion volumes obtained from MRI scans, including post-contrast T1Gd [7, 20, 52], are derived from a single MRI time point before treatment. In this work, we set a range for the data presented in [52] and perform investigations on this specific patient cohort. We confine our investigation to a numerical interval for invasion rates, ranging from 1.1542 to 7.2827, as specified in Table 1.

Table 1. D : net rate of invasion; ρ : net rate of proliferation; Surv. Days: Overall survival days; Censorship (1=censored): The term 'censored' signifies incomplete information, as the event (e.g., death or failure) did not occur within the study period or the patient was lost to follow-up.; The units are $D \sim \text{mm}^2/\text{year}$; $\rho \sim 1/\text{year}$

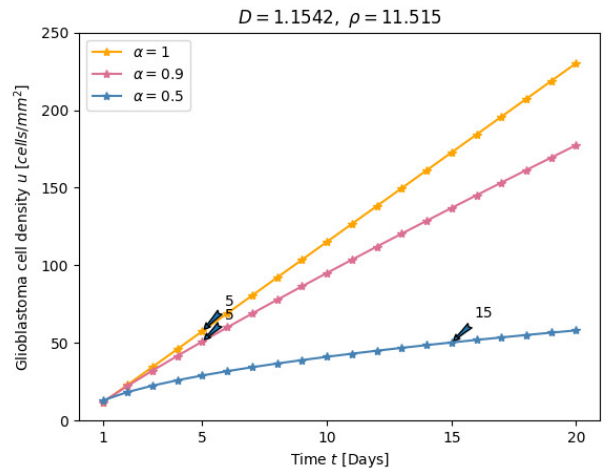
Patient	Gender	D	ρ	Surv. Days	Censorship
1	F	3.65	22.975	1292	0
2	F	1.1542	11.515	375	0
3	F	4.5951	22.975	65	0
4	F	7.2827	18.25	124	0
5	F	5.7849	14.496	115	0
6	M	2.303	36.414	126	0
7	M	4.5951	11.515	2139	1
8	M	7.2827	29.924	224	0
9	M	3.65	14.496	260	0
10	M	5.7849	9.1467	1143	0
Mean	-	4.60826	19.17067	586.3	-

The data presented in this table is sourced from Reference [52]

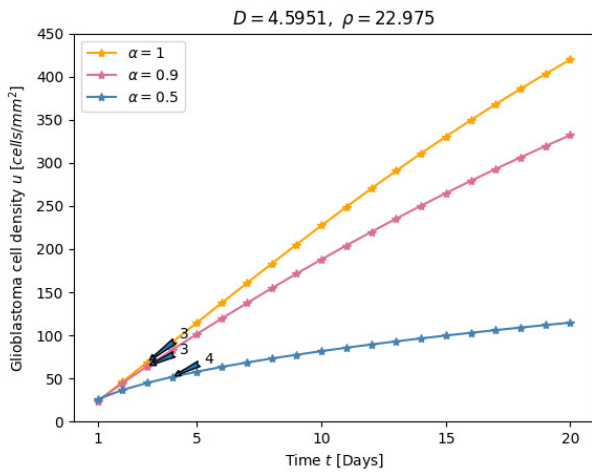
Considering the Caputo fractional derivative definition given by Definition 2, it is clear that directly assigning the derivative order of 1 to the model is not applicable. Taking into account Remark 1, it is seen that in the scenario where $\alpha = 1$, the numerical scheme (13) transitions into the classical numerical scheme. Therefore, we set one of the α values to 0.9 to facilitate observation of the approximation to the classical numerical scheme characterized by $\alpha = 1$. Accordingly, we execute the model individually for each patient, utilizing fractional derivative orders of $\alpha = 0.5$, $\alpha = 0.9$, and $\alpha = 1$ for the analyses. We place the peak of the Gaussian distribution given by (11) at the center of the domain.



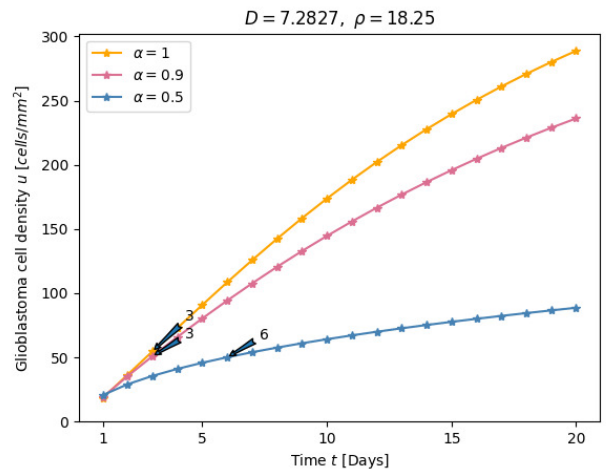
(a) Patient 1



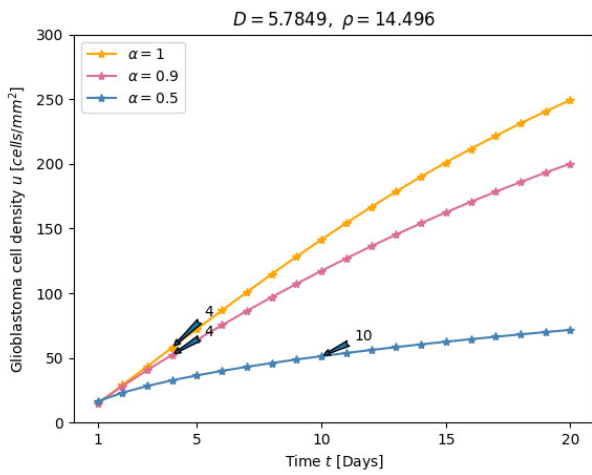
(b) Patient 2



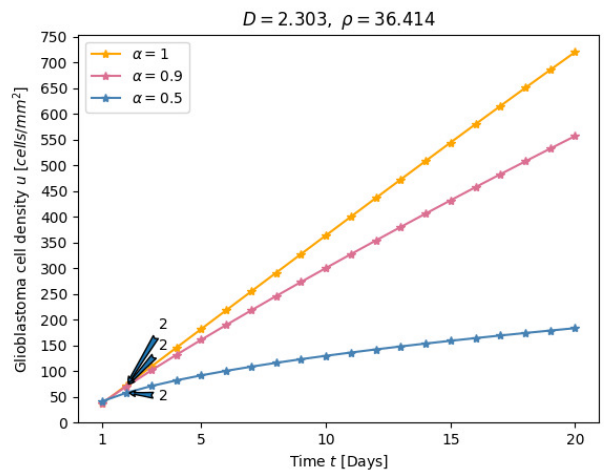
(c) Patient 3



(d) Patient 4



(e) Patient 5



(f) Patient 6

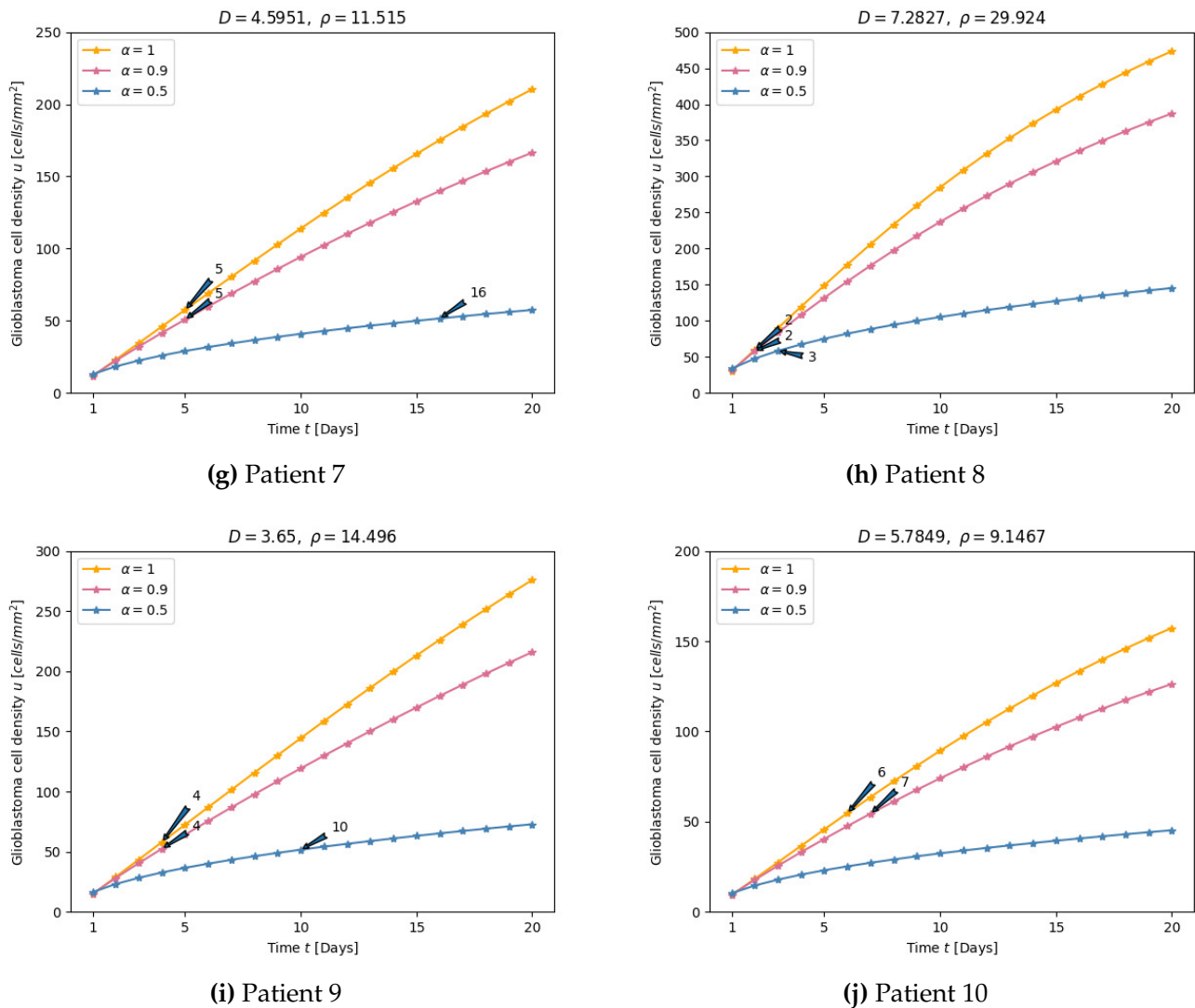


Figure 1. The maximum glioblastoma cell density observed each day over a twenty-day period under the three different derivative orders for each patient listed in Table 1 and the corresponding tumor visibility timing. Each small data point on the curves, depicted as asterisks, corresponds to consecutive days. Arrow symbols, along with corresponding numerical annotations, signify the days on which the tumor cell count achieved the threshold of 50 cells/mm² within the respective day. The term α represents the Caputo fractional derivative order

We keep both the initial cell density, $u_0 = 0.0147$, and the standard deviation, $\sigma = 2.86$ mm, in the Gaussian distribution constant, in accordance with [13, 14, 18, 19]. We hold the maximum cell carrying capacity of the tissue constant at $K = 10^8$ cells/mm³ for all simulations, consistent with [20]. We consider invasion and proliferation coefficients, denoted as D and ρ , respectively, as patient-specific values, as in Table 1. To execute the model, we employ the numerical scheme with a time step of $\tau = 0.01$, and a spatial discretization involving a domain length of 50 mm with 25 grid points. With the adjustments above, we generate daily glioblastoma cell densities for each patient over a twenty-day period, as demonstrated in Figure 1.

As a result, in Figure 1, the consideration of both proliferation rates and glioblastoma cell density values on the y -axes revealed a conspicuous trend, showcasing the dominance of proliferation rates in the model across all examined cases. Stated differently, the model notably initiated the generation of glioblastoma cell densities, with a specific focus on proliferation rates. This indicates that the tumor growth model may be an effective tool for tracking the temporal evolution of tumor

mass formation. Upon comparison of data from cases where each pair has the same proliferation rates, such as in the cases of Patients 1 and 3, Patients 2 and 7, or Patients 5 and 9, it was observed that a higher value of the invasion parameter slowed down the effect of the proliferation parameter. Accordingly, a slowdown in the growth rate of glioblastoma cell density was observed.

On the other hand, the numerical range identified in Table 1 for invasion parameter values, which comes from the data source, resulted in consistently smaller invasion rates than their proliferation counterparts in each case. Therefore, we now conduct an additional analysis to assess the dominance of the proliferation rate in the reverse case. To do this, we select arbitrary invasion and proliferation rates, namely, $D = 7.01$ and $\rho = 4.99$, while maintaining consistency with all other parameters and methodologies employed in the preceding analyses. Accordingly, we present a magnified visualization illustrating the early stages of glioblastoma cell density for the three distinct derivative orders of α , as shown in Figure 2.

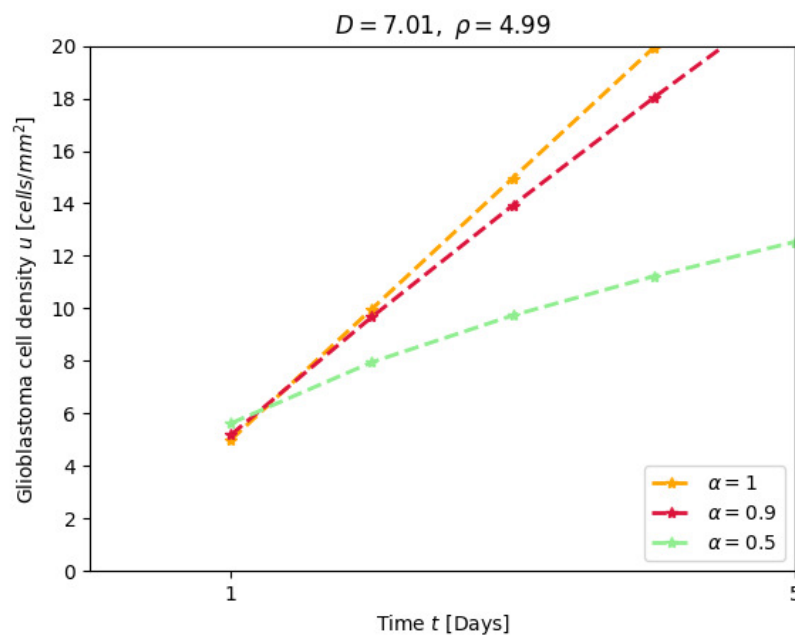


Figure 2. Magnified view of the initiation of glioblastoma cell density under the three different derivative orders of α with the arbitrary parameter values of D and ρ

For the arbitrary parameter values, it was clearly observed that glioblastoma initiation commences with a numerical value closely aligned with the proliferation rate, $\rho = 4.99$, for all three derivative orders of α , as shown in Figure 2. In conclusion, the proliferation rate being smaller than the invasion rate does not constitute a transformative factor influencing the dominance of the proliferative behavior in the model. Therefore, this analysis further underscores the tumor growth model's efficacy in capturing the process of glioblastoma mass formation.

Investigation of tumor visibility timing

The complexity of glioblastoma and its propensity for recurrence underscore the need for a nuanced understanding of its recurrence patterns for improved patient-specific management. In this section, we address this void and perform a patient-specific short-term follow-up to investigate the timing of glioblastoma cell visibility on MRI for the recurrence period. The analyses conducted in the preceding section emphasize the efficacy of the tumor growth model in

tracking the glioblastoma formation process, thereby affirming its ability to predict tumor visibility timing. In light of this finding, we proceed with our further discussions over the patient cohort presented in Table 1, which comprises ten patients newly diagnosed with glioblastoma.

Due to the invasive nature of glioblastoma, only a portion of the tumor can be detected with available medical imaging techniques. Examinations of computed tomography (CT) images and microscopic studies on postmortem brain slices indicate a detection threshold of $40,000 \text{ cells}/\text{cm}^2$ for advanced CT scans [23]. This threshold corresponds to approximately 400 cells in the approximately 1 mm^2 area covered by a 10x objective, or approximately 25 cells in the same area covered by a 40x objective for a histopathologist [21]. In this study, we adopt a threshold value of $50 \text{ cells}/\text{mm}^2$ as a threshold. For a histopathologist, this threshold may correspond to approximately 5 cells in an area covered by a $10\times$ objective, following [21]. Here, we conduct examinations assuming that all patients receive standard treatment. With the same numerical scheme adjustments as in the previous section, we consider a twenty-day recurrence period following standard treatment. As mentioned in Subsection 4 and illustrated in Figure 1, under the three specified α values, the maximum glioblastoma densities were generated, which were attained daily throughout the considered recurrence time frame. Then, we determine the days on which the $50 \text{ cells}/\text{mm}^2$ threshold was reached for each patient under the three derivative orders of α .

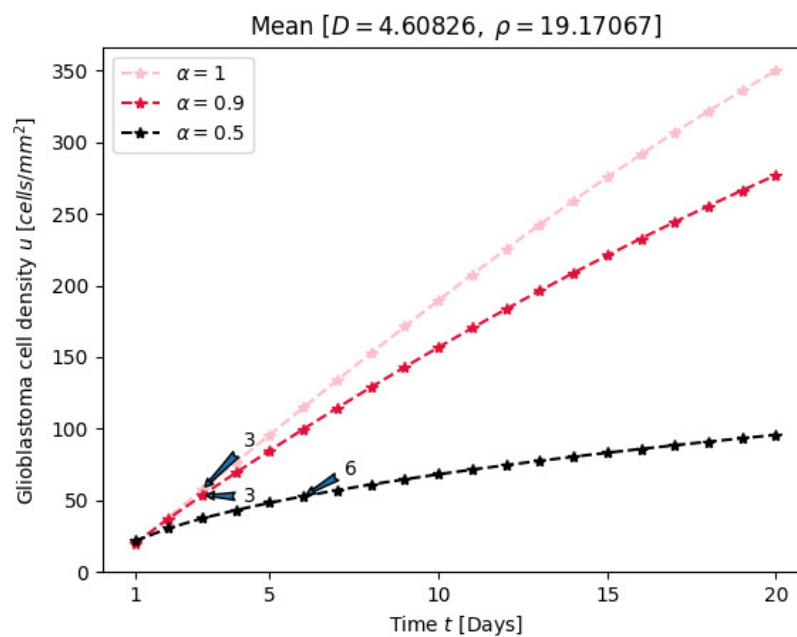


Figure 3. The maximum glioblastoma cell density observed each day over a twenty-day period under the three different derivative orders of α for the mean value and the corresponding tumor visibility timing

In conclusion, the classical derivative, defined by the order of $\alpha = 1$, depicted a growth pattern that rapidly reached the tumor visibility threshold of $50 \text{ cells}/\text{mm}^2$ in the initial time steps, exhibiting a rapid departure from this threshold. A similar trend was observed when choosing $\alpha = 0.9$ as a value close to the classical order. In contrast, when the fractional derivative order was set to $\alpha = 0.5$, the model showed a higher sensitivity to the tumor visibility threshold. That is, significant variations in the time for the tumor to reach the visibility threshold were observed for $\alpha = 0.5$ across the examined time span. Moreover, upon comparing Patient 2 and Patient 7, both exhibiting identical proliferation rates, it became evident that a higher invasion rate led to a delay in tumor visibility timing for $\alpha = 0.5$, unlike other derivative orders. In contrast to the remaining cases,

Patient 10, characterized by a comparatively lower proliferation rate and a higher invasion rate, it was observed that the tumor visibility threshold for $\alpha = 0.5$ was not reached in the relevant time period. However, given its proximity to the tumor visibility threshold on the twentieth day, it can be anticipated that the visibility threshold will likely be reached in the ensuing days. Consequently, analyses revealed that fractional derivatives model a more controlled growth behavior in contrast to the classical derivative.

It is notable that the tumor typically reached the 50 cells/mm^2 threshold within the same day for the derivative orders of $\alpha = 0.9$ and $\alpha = 1$, except for Patient 10. It is essential to elucidate that this does not necessarily denote the same cell count. Rather, this means that the glioblastoma densities exceeded the threshold on the specified day and manifested varied values beyond this threshold for both derivative orders.

As a final step, we investigate the timing of tumor visibility for the mean value of both invasion and proliferation rates presented in Table 1. As observed in Figure 3, the glioblastoma cell density surpassed the tumor visibility threshold within six days for the mean under all three distinct derivative orders of α . Given that the empirical evidence indicates the presence of glioma cells throughout the CNS within seven days following the implantation of tumors into a rat brain [21], our findings appear to be coherent with this observed phenomenon.

Investigation of tumor growth speed and survival correlation

As an additional experimental study, we examine the connection between patient survival and tumor growth speed for patients with glioblastoma in this part. To accomplish this, we employ a metric that considers the successive interday tumor growth speed. Here we consider a period from the initial diagnosis of glioblastoma to the day of death for the simulations. We use the numerical data extracted from [52], and presented in Table 2. To execute the model, we adopt identical parameter values as detailed in Subsection 4, with the exception of the time step, which is set to $\tau = 0.1$ with a fractional order of $\alpha = 0.5$.

Table 2. D : net rate of invasion; ρ : net rate of proliferation; Surv. Days: Overall survival days (from diagnosis to death); The units are $D \sim \text{mm}^2/\text{year}$; $\rho \sim 1/\text{year}$

Patient	Gender	D	ρ	Surv. Days
1	F	1.1542	11.515	375
2	F	1.8293	289.24	446
3	M	2.303	36.414	126
4	M	0.91684	5.7712	862

The data presented in this table is sourced from Reference [52]

We first explore the temporal trends of glioblastoma densities considering the survival duration of patients, as illustrated in Figure 4. When glioblastoma cell densities were examined, tumor growth trends within this group revealed the predominance of the proliferation term, as in the patient group discussed in Subsection 4. To further analyze the current growth trend for each patient, we apply a metric given by

$$\Delta \text{GCV}_k = u_{max}^{k+1} - u_{max}^k \tag{14}$$

where $k \in [1, S - 1]$. Here, S is the total number of survival days in the period after diagnosis, expressed as survival days in Table 2, u_{max} is the maximum cell density, and k is the time index. To reveal potential patterns among the patients, we apply metric (14) to the daily maximum glioblastoma cell densities obtained above, as visualized in Figure 5. In conclusion, the glioblas-

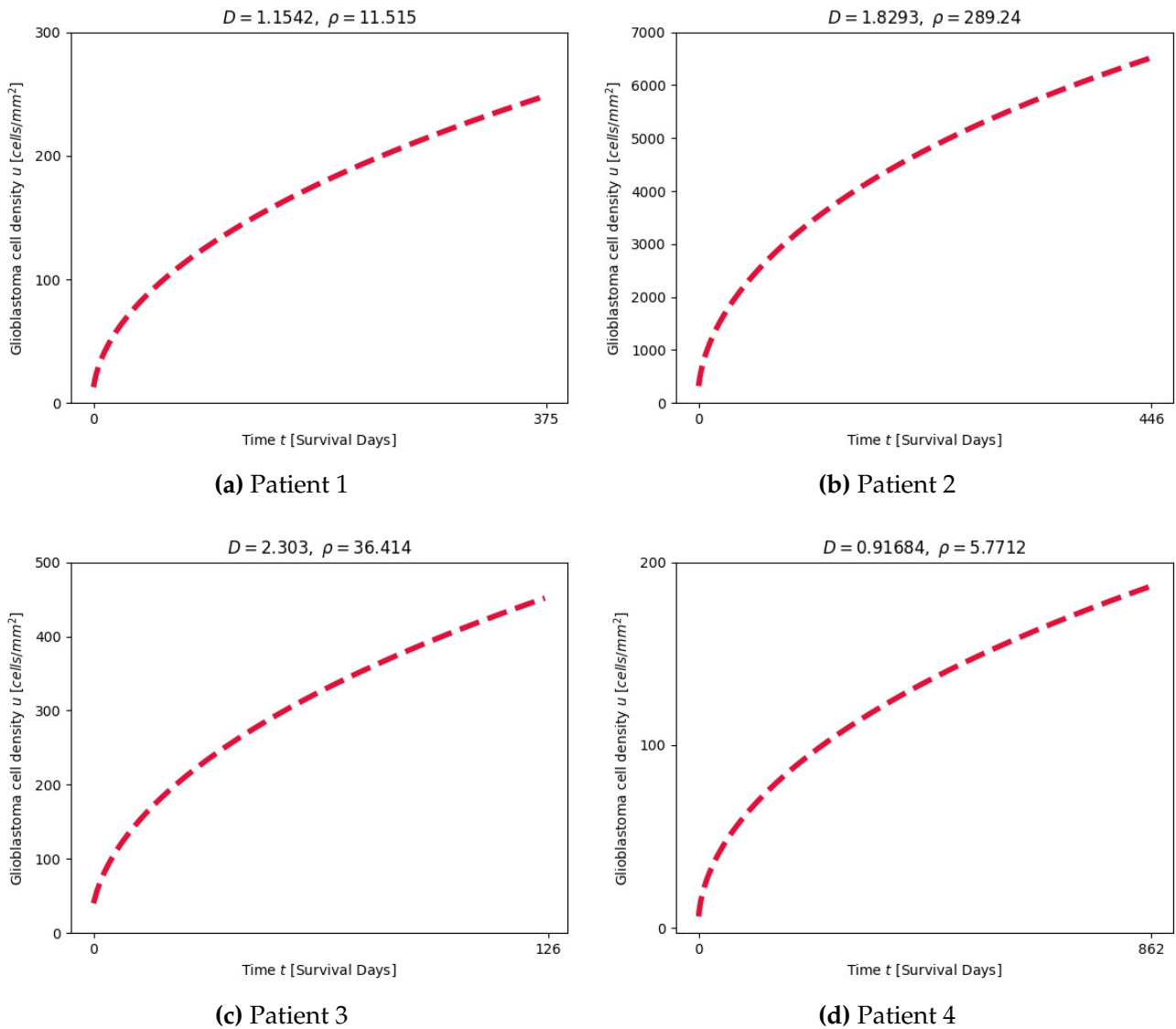


Figure 4. The maximum glioblastoma cell densities over the survival duration of patients listed in [Table 2](#)

toma cell densities exhibited a deceleration in growth speed when compared to the preceding days, as a specific pattern across four patients. This deceleration may be attributed to necrosis formation, indicating cell death within the tumor tissue, particularly given the dominance of the proliferation phenomenon in the model. To perform a patient-specific analysis of this change, we impose two arbitrary thresholds indexed to each patient's own tumor cell densities. These express two criteria of the form $T1 = 0.20\max(\Delta GCV_k)$ and $T2 = 0.06\max(\Delta GCV_k)$. We then determine the first days when the glioblastoma cell variation, ΔGCV_k , fell below these thresholds for each patient. When reviewing the outcomes, it was observed that in the case of Patient 1, death ensued relatively quickly after the ΔGCV_k value fell below the second threshold, $T2$, while in the cases of Patients 2 and 4, death occurred much later. In contrast, in the instance of Patient 3, death was noted after the ΔGCV_k value fell below the first threshold, $T1$, before attaining the second threshold, $T2$. Consequently, no remarkable patterns were observed linking the thresholds to the glioblastoma cell variation during the survival days. We also examine the final delta values of the patients, as shown in [Figure 6](#). The values displayed on the y -axis in [Figure 6](#) correspond to the final delta values for the two days preceding the occurrence of death. In conclusion, the examined patient cohort did not exhibit any significant patterns in this temporal window. How-

ever, these conclusions further corroborated the long-recognized yet unexplained heterogeneity in inter-patient variability among glioblastoma cases, as mentioned in [53, 54].

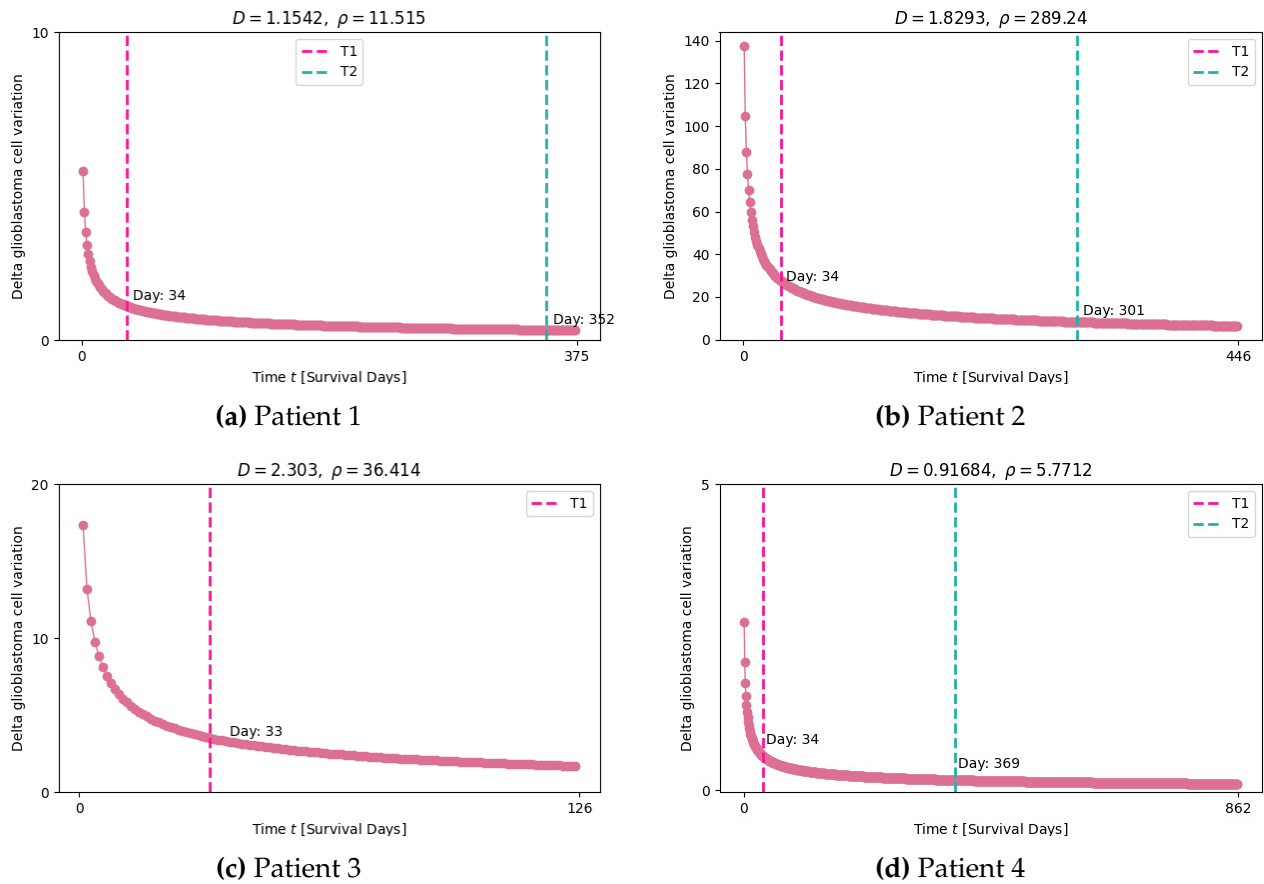


Figure 5. Correlation of glioblastoma cell variation with patient survival under the fractional order of $\alpha = 0.5$. Each pink marker on the curves signifies the values commencing from the initial delta, ΔGCV_1 , which corresponds to the first two days after diagnosis, extending to the final delta value, ΔGCV_{S-1} , representing the consecutive two days before mortality. The pink dotted line denotes the first threshold, $T1$, representing the point at which the ΔGCV_k value reaches %20 of the maximum value of ΔGCV_k . Similarly, the sea green dotted line delineates the second threshold, $T2$, symbolizing the point at which the ΔGCV_k value reaches %6 of the maximum value of ΔGCV_k . The days marked in black adjacent to the dotted lines signify the initiation of these events

5 Discussion

In this work, we use an explicit fractional finite difference scheme for the simulations. In addition to the established stability issues associated with explicit schemes, it is noteworthy that the inclusion of fractional derivatives in the employed numerical scheme introduced an additional layer of complexity to this challenging scenario. In cases not included in this study but defined with relatively larger invasion rates, difficulties were encountered in managing these high values. The applied fractional numerical scheme faced challenges in handling a wider range of invasion parameter values, particularly for values below the fractional order $\alpha = 0.5$, which serves as the lower limit in the investigative scope of this study. To address these challenges, a finer-scale temporal discretization strategy was employed. However, this adjustment resulted in a significant escalation of computational time with simulations extending up to thirty-six hours. These findings recommended the adoption of implicit methods in future studies as a prudent and feasible strategy

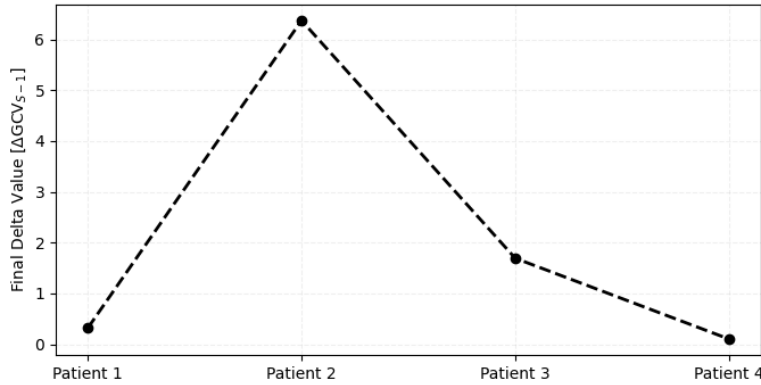


Figure 6. The values of the final delta, ΔGCV_{S-1} , for the patients listed in [Table 2](#)

to mitigate computational time and efficiently handle extensive numerical data. By this means, it appears possible to leverage the subtle effects of smaller fractional orders across a broad range of parameter values.

Upon theoretical evaluation of the decrease in the speed of increase in maximum cell densities for each day over the survival period discussed in Subsection 4, it can be inferred that the observed deceleration reflects convergence behavior to a singular point in the proliferation term, $f(u)$. However, this deceleration may be attributed to necrosis formation, which signifies cell death in the tumor tissue, particularly when considering the dominance of the proliferation phenomenon in the model. Examining the growth model's ability to effectively capture necrosis occurrences would have been facilitated with more detailed information about the studied patient cohort. Regrettably, this study was unable to access such detailed data. Future research endeavors are anticipated to provide opportunities for more comprehensive analysis in this regard. In the context of the final experiments, the ΔGCV_k value for all four patients fell below the initial threshold, $T1$, on nearly the same days, as illustrated in [Figure 5](#). This is attributable to the proximate invasion rates observed across the cases. Working with patient data characterized by higher invasion rates may lead to variability in this regard.

Overall, the findings presented in this study should be contextualized within the scope of experimental investigations conducted through a mathematical equation. To transparently evaluate the advantages of the proposed growth model, conducting rigorous assessments involving clinical validations, such as *in vivo* or *in vitro*, would be highly enlightening. To the best of our knowledge, our growth model, even in its classical form has not been explored in the context of cancer research. This suggests the model's potential as a focal point for future cancer investigations within the realm of mathematical modeling.

6 Conclusion

In this work, we introduced a mathematical model to investigate glioblastoma growth at a macroscopic scale, presenting a structure that incorporates a calibration criterion based on fractional derivatives. The findings highlighted the importance of incorporating fractional derivatives in refining mathematical models to better capture real-life observations. The analyses strongly revealed the dominance of the proliferation phenomenon in the proposed growth model, suggesting its robustness as a tool for tracking glioblastoma mass formation and predicting the timing of tumor visibility on MRI during recurrence follow-up. Estimates of tumor visibility timing, conducted with consideration for three distinct derivative orders, pointed towards a more controlled approach with small fractional derivative orders. The obtained findings regarding tumor visibility

timing exhibited consonance with the empirical observations, reinforcing the validity of our methodology. The analyses of the relationship between patient survival and tumor growth speed, utilizing the growth model developed in this research, further substantiated the well-established, yet inexplicable, variations in inter-patient variability for glioblastoma cases.

Declarations

Use of AI tools

The authors declare that they have not used Artificial Intelligence (AI) tools in the creation of this article.

Data availability statement

All data generated or analyzed during this study are included in this article.

Ethical approval

Not applicable

Consent for publication

Not applicable

Conflicts of interest

The authors declare that they have no conflict of interest.

Funding

Not applicable

Author's contributions

N.K.: Conceptualization, Methodology, Investigation, Visualization, Writing-Original draft preparation, Software, Validation, Writing-Reviewing and Editing. N.Ö.: Supervision. All authors have read and agreed to the submitted version of the manuscript.

Acknowledgements

This work was supported by the Scientific and Technological Research Council of Türkiye (TUBITAK) (Grant No. E-21514107-115.99-301087). The authors would like to thank the anonymous reviewers for their valuable comments and suggestions, which have enhanced the quality of the manuscript.

References

- [1] Yabo, Y.A., Niclou, S.P. and Golebiewska, A. Cancer cell heterogeneity and plasticity: a paradigm shift in glioblastoma. *Neuro-Oncology*, 24(5), 669-682, (2022). [[CrossRef](#)]
- [2] Louis, D.N., Perry, A., Wesseling, P., Brat, D.J., Cree, I.A., Figarella-Branger, D. et al. The 2021 WHO classification of tumors of the central nervous system: a summary. *Neuro-Oncology*, 23(8), 1231-1251, (2021). [[CrossRef](#)]
- [3] Carlsson, S.K., Brothers, S.P. and Wahlestedt, C. Emerging treatment strategies for glioblastoma multiforme. *EMBO Molecular Medicine*, 6(11), 1359-1370, (2014). [[CrossRef](#)]
- [4] Kelley, P.J. and Hunt, C. The limited value of cytoreductive surgery in elderly patients with malignant gliomas. *Neurosurgery*, 34(1), 62-67, (1994).

- [5] Piroth, M.D., Pinkawa, M., Holy, R., Klotz, J., Schaar, S., Stoffels, G. et al. Integrated boost IMRT with FET-PET-adapted local dose escalation in glioblastomas. *Strahlentherapie und Onkologie*, 188(4), 334-339, (2012). [[CrossRef](#)]
- [6] Silbergeld, D.L. and Chicoine, M.R. Isolation and characterization of human malignant glioma cells from histologically normal brain. *Journal of Neurosurgery*, 86(3), 525-531, (1997). [[CrossRef](#)]
- [7] Harpold, H.L.P., Alvord Jr, E.C. and Swanson, K.R. The evolution of mathematical modeling of glioma proliferation and invasion. *Journal of Neuropathology & Experimental Neurology*, 66(1), 1-9, (2007). [[CrossRef](#)]
- [8] Pandya, N.M., Dhalla, N.S. and Santani, D.D. Angiogenesis-a new target for future therapy. *Vascular Pharmacology*, 44(5), 265-274, (2006). [[CrossRef](#)]
- [9] Das, S. *Functional Fractional Calculus for System Identification and Controls*. Springer: New York, (2008). [[CrossRef](#)]
- [10] Curtin, L., Whitmire, P., White, H., Bond, K.M., Mrugala, M.M., Hu, L.S. et al. Shape matters: morphological metrics of glioblastoma imaging abnormalities as biomarkers of prognosis. *Scientific Reports*, 11(1), 23202, (2021). [[CrossRef](#)]
- [11] Konukoglu, E., Clatz, O., Bondiau, P.Y., Delingette, H. and Ayache, N. Extrapolating glioma invasion margin in brain magnetic resonance images: suggesting new irradiation margins. *Medical Image Analysis*, 14(2), 111-125, (2010). [[CrossRef](#)]
- [12] Burgess, P.K., Kulesa, P.M., Murray, J.D. and Alvord Jr, E.C. The interaction of growth rates and diffusion coefficients in a three-dimensional mathematical model of gliomas. *Journal of Neuropathology & Experimental Neurology*, 56(6), 704-713, (1997). [[CrossRef](#)]
- [13] Jacobs, J., Rockne, R.C., Hawkins-Daarud, A.J., Jackson, P.R., Johnston, S.K., Kinahan, P. et al. Improved model prediction of glioma growth utilizing tissue-specific boundary effects. *Mathematical Biosciences*, 312, 59-66, (2019). [[CrossRef](#)]
- [14] Jbabdi, S., Mandonnet, E., Duffau, H., Capelle, L., Swanson, K.R., Pelegrini-Issac, M. et al. Simulation of anisotropic growth of low-grade gliomas using diffusion tensor imaging. *Magnetic Resonance in Medicine*, 54(3), 616-624, (2005). [[CrossRef](#)]
- [15] Konukoglu, E., Clatz, O., Menze, B.H., Stieltjes, B., Weber, M.A., Mandonnet, E. et al. Image guided personalization of reaction-diffusion type tumor growth models using modified anisotropic eikonal equations. *IEEE Transactions on Medical Imaging*, 29(1), 77-95, (2010). [[CrossRef](#)]
- [16] Le, M., Delingette, H., Kalpathy-Cramer, J., Gerstner, E.R., Batchelor, T., Unkelbach, J. et al. MRI based Bayesian personalization of a tumor growth model. *IEEE Transactions on Medical Imaging*, 35(10), 2329-2339, (2016). [[CrossRef](#)]
- [17] Lipkova, J., Angelikopoulos, P., Wu, S., Alberts, E., Wiestler, B., Diehl, C. et al. Personalized radiotherapy design for glioblastoma: integrating mathematical tumor models, multimodal scans, and Bayesian inference. *IEEE Transactions on Medical Imaging*, 38(8), 1875-1884, (2019). [[CrossRef](#)]
- [18] Rockne, R., Alvord Jr, E.C., Reed, P.J. and Swanson, K.R. Modeling the growth and invasion of gliomas, from simple to complex: the goldie locks paradigm. *Biophysical Reviews and Letters*, 03(01n02), 111-123, (2008). [[CrossRef](#)]
- [19] Rockne, R., Alvord Jr, E.C., Rockhill, J.K. and Swanson, K.R. A mathematical model for brain tumor response to radiation therapy. *Journal of Mathematical Biology*, 58, 561-578, (2009).

[CrossRef]

- [20] Rockne, R., Rockhill, J.K., Mrugala, M., Spence, A.M., Kalet, I., Hendrickson, K. et al. Predicting the efficacy of radiotherapy in individual glioblastoma patients in vivo: a mathematical modeling approach. *Physics in Medicine and Biology*, 55(12), 3271-3285, (2010). [CrossRef]
- [21] Swanson, K.R., Alvord Jr, E.C. and Murray, J.D. A quantitative model for differential motility of gliomas in grey and white matter. *Cell Proliferation*, 33(5), 317-329, (2000). [CrossRef]
- [22] Swanson, K.R., Bridge, C., Murray, J.D. and Alvord Jr, E.C. Virtual and real brain tumors: using mathematical modeling to quantify glioma growth and invasion. *Journal of the Neurological Sciences*, 216(1), 1-10, (2003). [CrossRef]
- [23] Tracqui, P., Cruywagen, G.C., Woodward, D.E., Bartoo, G.T., Murray, J.D. and Alvord Jr, E.C. A mathematical model of glioma growth: the effect of chemotherapy on spatio-temporal growth. *Cell Proliferation*, 28(1), 17-31, (1995). [CrossRef]
- [24] Woodward, D.E., Cook, J., Tracqui, P., Cruywagen, G.C., Murray, J.D. and Alvord Jr, E.C. A mathematical model of glioma growth: the effect of extent of surgical resection. *Cell Proliferation*, 29(6), 269-288, (1996). [CrossRef]
- [25] Ucar, E., Ozdemir, N. and Altun, E. Fractional order model of immune cells influenced by cancer cells. *Mathematical Modelling of Natural Phenomena*, 14(3), 308, (2019). [CrossRef]
- [26] Ozdemir, N., Ucar, S. and Eroglu, B.B.I. Dynamical analysis of fractional order model for computer virus propagation with kill signals. *International Journal of Nonlinear Sciences and Numerical Simulation*, 21(3-4), 239-247, (2020). [CrossRef]
- [27] Ozkose, F., Yilmaz, S., Yavuz, M., Ozturk, I., Senel, M.T., Bagci, B.S. et al. A fractional modeling of tumor-immune system interaction related to Lung cancer with real data. *The European Physical Journal Plus*, 137, 1-28, (2022). [CrossRef]
- [28] Rahman, M., Arfan, M. and Baleanu, D. Piecewise fractional analysis of the migration effect in plant-pathogen-herbivore interactions. *Bulletin of Biomathematics*, 1(1), 1-23, (2023). [CrossRef]
- [29] Mustapha, U.T., Ado, A., Yusuf, A., Qureshi, S. and Musa, S.S. Mathematical dynamics for HIV infections with public awareness and viral load detectability. *Mathematical Modelling and Numerical Simulation with Applications*, 3(3), 256-280, (2023). [CrossRef]
- [30] Kawarada, H. On solutions of Initial-Boundary Problem for $u_t = u_{xx} + 1/(1-u)$. *Publications of the Research Institute for Mathematical Sciences*, 10(3), 729-736, (1975). [CrossRef]
- [31] Acker, A. and Walter, W. On the global existence of solutions of parabolic differential equations with a singular nonlinear term. *Nonlinear Analysis, Theory, Methods and Applications*, 2(4), 499-504, (1978). [CrossRef]
- [32] Ke, L. and Ning, S. Quenching for degenerate parabolic equations. *Nonlinear Analysis*, 34, 1123-1135, (1998).
- [33] Levine, H.A. and Montgomery, J.T. The quenching of solutions of some nonlinear parabolic equations. *SIAM Journal on Mathematical Analysis*, 11(5), 842-847, (1980). [CrossRef]
- [34] Levine, H.A. Levine, The phenomenon of quenching: a survey Trends in the theory and practice of nonlinear analysis. In Proceedings, *Sixth International Conference on Document Analysis and Recognition* (Vol. 110) pp. 275-286, North-Holland, Amsterdam, (1985).
- [35] Levine, H.A. Quenching, nonquenching, and beyond quenching for solution of some parabolic equations. *Annali di Matematica Pura ed Applicata*, 155, 243-260, (1989). [CrossRef]
- [36] Deng, K. and Levine, H.A. On the blow up of u_t at quenching. In Proceedings *American*

Mathematical Society, pp. 1049-1056, 106(4), (1989, August).

- [37] Guo, J.S. On the quenching behavior of the solution of a semilinear parabolic equation. *Journal of Mathematical Analysis and Applications*, 151, 58-79, (1990).
- [38] de Pablo, A., Quiros, F. and Rossi, J.D. Nonsimultaneous quenching. *Applied Mathematics Letters*, 15(3), 265-269, (2002). [[CrossRef](#)]
- [39] Ji, R., Zhou, S. and Zheng, S. Quenching behavior of solutions in coupled heat equations with singular multi-nonlinearity. *Applied Mathematics and Computation*, 223, 401-410, (2013). [[CrossRef](#)]
- [40] Jia, Z., Yang, Z. and Wang, C. Non-simultaneous quenching in a semilinear parabolic system with multi-singular reaction terms. *Electronic Journal of Differential Equations*, 2019(100), 1-13, (2019).
- [41] Mu, C., Zhou, S. and Liu, D. Quenching for a reaction-diffusion system with logarithmic singularity. *Nonlinear Analysis: Theory, Methods & Applications*, 71(11), 5599-5605, (2009). [[CrossRef](#)]
- [42] Zheng, S. and Wang, W. Non-simultaneous versus simultaneous quenching in a coupled nonlinear parabolic system. *Nonlinear Analysis: Theory, Methods & Applications*, 69(7), 2274-2285, (2008). [[CrossRef](#)]
- [43] Xu, Y. and Zheng, Z. Quenching phenomenon of a time-fractional diffusion equation with singular source term. *Mathematical Methods in the Applied Sciences*, 40(16), 5750-5759, (2017). [[CrossRef](#)]
- [44] Xu, Y. and Wang, Z. Quenching phenomenon of a time-fractional Kawarada equation. *Journal of Computational and Nonlinear Dynamics*, 13(10), 101010, (2018). [[CrossRef](#)]
- [45] Kilbas, A.A., Srivastava, H.M. and Trujillo, J.J. *Theory and Applications of Fractional Differential Equations* (Vol. 204). Elsevier: Amsterdam, (2006).
- [46] Oldham, K.B. and Sparriier, J. *The Fractional Calculus*. Academic Press, New York-London, (1974).
- [47] Podlubny, I. *Fractional Differential Equations*. Academic Press: San Diego, (1999).
- [48] Samko, S.G., Kilbas, A.A. and Marichev, O.I. *Fractional Integrals and Derivatives: Theory and Applications*. Gordon and Breach Science Publishers, Switzerland, (1993).
- [49] Du, M., Wang, Z. and Hu, H. Measuring memory with the order of fractional derivative. *Scientific Reports*, 3, 3431, (2013). [[CrossRef](#)]
- [50] Caputo, M. *Elasticità e Dissipazione*. Bologna: Zanichelli, (1969).
- [51] Caputo, M. and Mainardi, F. A new dissipation model based on memory mechanism. *Pure and Applied Geophysics*, 91, 134-147, (1971).
- [52] Yang, W., Warrington, N.M., Taylor, S.J., Whitmire, P., Carrasco, E., Singleton, K.W. et al. Sex differences in GBM revealed by analysis of patient imaging, transcriptome, and survival data. *Science Translational Medicine*, 11(473), eaao5253, (2019). [[CrossRef](#)]
- [53] Bi, J., Khan, A., Tang, J., Armando, A.M., Wu, S., Zhang, W. et al. Targeting glioblastoma signaling and metabolism with a re-purposed brain-penetrant drug. *Cell Report*, 37, 109957, (2021). [[CrossRef](#)]
- [54] Skaga, E., Kuleskiy, E., Fayzullin, A., Sandberg, C.J., Potdar, S., Kyttälä, A. et al. Intertumoral heterogeneity in patient-specific drug sensitivities in treatment-naïve glioblastoma. *BMC Cancer*, 19, 628, (2019). [[CrossRef](#)]

Mathematical Modelling and Numerical Simulation with Applications (MMNSA)
(<https://dergipark.org.tr/en/pub/mmnsa>)



Copyright: © 2024 by the authors. This work is licensed under a Creative Commons Attribution 4.0 (CC BY) International License. The authors retain ownership of the copyright for their article, but they allow anyone to download, reuse, reprint, modify, distribute, and/or copy articles in MMNSA, so long as the original authors and source are credited. To see the complete license contents, please visit (<http://creativecommons.org/licenses/by/4.0/>).

How to cite this article: Kar, N. & Özalp, N. (2024). A fractional mathematical model approach on glioblastoma growth: tumor visibility timing and patient survival. *Mathematical Modelling and Numerical Simulation with Applications*, 4(1), 66-85. <https://doi.org/10.53391/mmnsa.1438916>